NUMERICAL SIMULATION OF PULSATILE FLOW THROUGH STENOTIC VESSELS

Sonu S. Varghese, Steven H. Frankel
School of Mechanical Engineering,
Purdue University
West Lafayette, IN, USA 47907
sonusv@ecn.purdue.edu,frankel@ecn.purdue.edu

Robin Pitt, Spencer J. Sherwin
Department of Aeronautics
Imperial College of Science, Technology and Medicine
London, UK
robin.pitt@imperial.ac.uk,s.sherwin@ic.ac.uk

ABSTRACT

High-order simulations of pulsatile flow through a stenotic vessel were performed using the spectral/*hp* element method to study the post-stenotic flow field and the influence of fluid dynamic variables in the initiation of atherosclerosis. Asymmetric flow features were found to occur downstream of the stenosis, producing fluctuating regions of wall shear stress. Particle tracking was also employed to qualitatively study vorticity evolution. Mixing between core flow and near-wall structures was observed far downstream of the stenosis, away from the jet-like region which could promote cyclic transition to turbulence.

Steady flow simulations through elliptic and asymmetric stenosis models were also performed to assess the role of stenosis morphology on post-stenotic flow behavior. The geometry of the stenosis greatly affects the flow downstream, including the extent of mixing between the core and near-wall structures.

INTRODUCTION

Atherosclerosis, which is a process of progressive thickening and hardening of the walls of medium-sized and large arteries, is responsible for much coronary artery disease and strokes. Atherosclerotic plaques tend to be localized at sites of branching and artery curvature, and since complex flow patterns would be expected at these locations, fluid mechanics has played an important role in studying its initiation. When arteries become severely diseased, plaque develops to such a point that the arterial lumen becomes locally restricted, resulting in a stenosis.

Stenotic flows involve low Reynolds number, pulsatile flow through a restriction (most resembling a converging-diverging nozzle in the idealized case) featuring flow separation, strong shear layers, recirculation and reattachment. Classical experiments of flow through stenotic vessels have shown flow disturbances in the post-stenotic region (distal to the stenosis) causing highly fluctuating wall shear stress (WSS) levels (Ahmed and Giddens, 1984). Low, oscillatory shear stresses have been implicated in the development of atherosclerotic plaque. Due to the difficulties involved in making in vivo measurements, computational fluid dynamics (CFD) has recently begun to play a larger role in the study of stenotic flows. In the current study, we are performing three-dimensional computations of pulsatile flow through stenosed vessels at physiologically relevant Reynolds numbers. The objective is to study post-stenotic (distal) flow behavior and its effect on hemodynamic factors that promote atherogenesis.

METHODOLOGY

Three-dimensional numerical studies of stenotic flows were performed using the spectral/*hp* element method. The method provides high-order polynomial approximations to the Navier-Stokes equations on unstructured and hybrid meshes, which were used for this study to discretize the stenosis model. The meshing ensured sufficient resolution by performing a curvature based refinement algorithm upon cubic spline surfaces used to define the geometry. These surfaces then provided the surface definition used in the flow solver NEKTAR, which was used to numerically integrate the non-dimensional form of the Navier-Stokes equations (Karniadakis and Sherwin, 1999). Three different stenosis models were studied with the local stenosis shapes being described as circular, elliptic and asymmetric as shown in Figure 1. The curve defining the stenosis shapes was generated by a cosine function, similar to that used by Khalifa and Giddens (1981).

Pulsatile flow through a 60% (by area reduction) circular stenosis was simulated at a mean Reynolds number (Re) of 200, based on mean velocity. The analytical solution for fully developed pulsatile flow in a circular pipe, as proposed by Womersley (1955) is:

$$u(r,t) = -\frac{iP}{\omega\rho}\left(\frac{1 - J_0\left(i^{\frac{3}{2}}\alpha\frac{r}{a}\right)}{J_0\left(i^{\frac{3}{2}}\alpha\right)}\right)\exp(i\omega t) \qquad (1)$$

where a is the pipe radius, $J_0()$ is the Bessel function of type 0, ω the angular frequency of the pulsation, P the pressure gradient and ρ the density. α is the non-dimensional Womersley number:

$$\alpha = a\sqrt{\frac{\omega}{\nu}} \qquad (2)$$

with ν kinematic viscosity. The Womersley number for the simulation was 7.16. An inflow velocity of the form of (1)

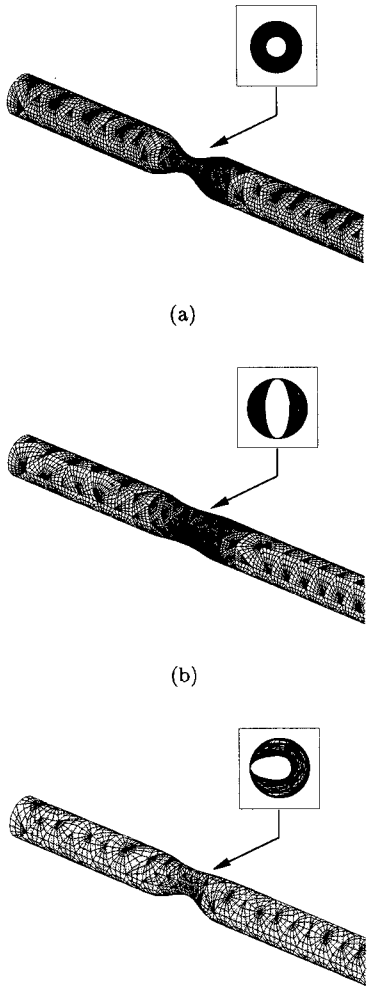

Figure 1: Geometry and higher order mesh for the stenosis models. Only a portion of the whole model is shown and the stenosis shapes are indicated for the (a) circular, (b) elliptic, and (c) asymmetric cases, respectively.

corresponding to a time periodic flow rate given by:

$$Q(t) = 1 + 0.75\sin(\omega t) \tag{3}$$

was prescribed.

Steady flow through the elliptic and asymmetric stenosis models was also simulated, at a Reynolds number of 500, based on mean velocity. For these cases, fully developed pipe flow was specified at the inlet as:

$$u(x, y) = 1 - 4(x^2 + y^2) \tag{4}$$

In all simulations, the outflow had constant sectional pressure and zero normal derivatives on the velocity.

Doorly et al (2002) obtained a qualitative physical model for the evolution of flow vorticity and the generation of vortex structures by tracking material lines aligned with the vorticity vector over distances sufficiently small for viscous dissipation and boundary vorticity flux to be neglected. Using two marker material rings, one closer to the axis and the other near the wall, differences in vorticity evolution at various locations can be tracked. Stretching of these rings would imply an increase in the vorticity. Doorly et al have suggested that for pipe flow, a ring of material particles with radius $\frac{3}{4}$ that of the pipe, is a reasonable choice to track the evolution of mean vorticity near the walls, while a ring with radius $\frac{1}{4}$ that of the pipe, could be used to visualize core flow behavior. The method also indicates some aspects of mixing in the vessel. A high order Lagrangian particle tracking routine was applied to the results as described by Coppola et al (2001).

RESULTS

Figures 2 and 3 show axial velocity profiles and contours obtained during different phases of pulsatile flow through the circular stenosis at different axial stations downstream of the stenosis center (throat). The velocity profiles show the flow accelerating through the stenosis with the maximum occuring during peak flow conditions at the inlet. During the acceleration phase, flow separation starts to occur in the immediate downstream vicinity of the stenosis with flow reattachment occuring around 5 diameters downstream of the stenosis. Towards the end of acceleration, at peak flow, these separation zones grow asymmetrically and in-plane velocity vectors show a swirling motion of the fluid breaking the coherence of the stenotic jet between 5 and 7 diameters downstream of the stenosis throat. During deceleration, the adverse pressure gradient promotes further flow separation and assymetries become more pronounced, as fairly large negative velocity regions exist in a large portion of the downstream region. Jet breakdown and flow reattachment moves further downstream to about 11 diameters away from the throat at minimum flow. As we move back into the acceleration phase, the flow becomes mostly positive once again.

Figure 4 illustrates trajectories of material rings released during different phases of the pulsatile cycle. During acceleration, the inner ring, which indicates how the the core flow behaves, has little vorticity and simply travels right through the vessel without distorting too much unlike the flow closer to the walls. The larger ring undergoes rapid stretching and folding in the streamwise direction after it passes through the stenosis and continues to distort, eventually dominating much of the downsteam section of the vessel, which is also the case during peak flow. However under peak flow conditions, the inner ring can be seen to deform and stretch more than the earlier case, indicating increasing axial vorticity in the downstream region during this time.

Trajectories of material rings released during the deceleration phase show a different pattern than those released during the acceleration phase and peak flow, as can be seen in Figure 3(c). Here, the inner ring initially undergoes rapid stretching and folding in a manner similar to the outer rings in the previous cases indicating intensifying axial vorticity in the core flow, though this takes place much further downstream. At these locations, evolution of the material rings indicates some degree of mixing between the distorted inner and outer rings. This mixing between the core flow and the near wall structures could be responsible for cyclic transition to turbulence far downstream from the stenosis. As we move back into the acceleration phase, the extent of distortion and mixing of the rings is less.

Axial velocity contours and corresponding in-plane velocity vectors for steady flow through the elliptic stenosis in Figure 5 shows the flow accelerating symmetrically through the stenosis forming an elliptic jet, with separation occuring immediately downstream of the stenosis. Asymmetric

separation regions on either side of the stenotic jet grow and fade until about 9 diameters downstream of the throat, after which the flow is mostly positive and symmetric. Material line trajectories for this case are shown in Figure 6. Both rings deform in an almost symmetric manner across the stenosis before the outer ring undergoes rapid stretching and folding in the axial direction. Evidently, for this case of steady flow at Reynolds number of 500, there is no mixing between the simultaneously released core and outer rings.

In the case of the asymmetric stenosis, the flow accelerates preferentially across the stenosis as shown in Figure 7 with flow separation occuring downstream similar to the earlier cases. The flow becomes increasingly asymmetric further away from the throat region with jet breakdown occuring between 7 and 11 diameters downstream of the throat. Particle ring trajectories for this case are very different from those obtained for its elliptic counterpart, as illustrated in Figure 8. Again, the core flow can be seen to accelerate preferentially across the narrow stenosis region before increased stretching and folding in the downstream section. Asymmetric distortion of the outer ring also occurs and some degree of mixing is observed far downstream, away from the jet-like region in the immediate vicinity of the stenosis.

DISCUSSION AND CONCLUSIONS

Three-dimensional numerical simulations of pulsatile flow through stenotic vessels were performed using the high-order spectral/*hp* element method. Results for pulsatile flow through the circular stenosis show highly disturbed flow in the downstream section of the vessel, away from the stenosis throat. The continuously evolving asymmetric regions of flow separation in the downstream flow field can cause high temporal and spatial variations of wall shear stress, both of which can stimulate the atherogenesis process even further, since cells at these locations would experience highly oscillatory shear stress levels. Evolution of material particle rings released during the deceleration phase, in the presence of an adverse pressure gradient, show the core flow experiencing increasing levels of vorticity along with some degree of mixing between the near-wall and core flow structures. This could promote transition to turbulence during certain phases of the cycle, thereby influencing reversed flow and separation regions and controlling the mixing of particles across the vessel section.

The flow patterns obtained from the results of the steady flow calculations, through the elliptic and asymmetric stenoses, indicate that stenosis morphology plays a large role in influencing post-stenotic flow behavior. While material line trajectories showed that the core flow and near-wall structures do not interact for the elliptic case, highly asymmetric flow develops after the asymmetric stenosis with some degree of mixing taking place as well. Asymmetric flow separation downstream of the stenosis throat also results in stagnated and reversed wall shear stress levels promoting the growth of atherosclerotic plaque.

The spectral/*hp* element method, utilized for the present computations, is a powerfool tool to investigate stenotic flows, due to the ability to perform high-order computations over complex domains. Analysis techniques, such as the Lagrangian particle tracking employed here, can also go a long way in providing a better understanding of the flow physics involved.

REFERENCES

Ahmed, S., Giddens, D.P., 1984, "Pulsatile Poststenotic Flow Studies with Laser Doppler Anemometry", ' *Journal of Biomechanics*, Vol. 17, pp. 695-705.

Coppola, G., Sherwin, S.J., Peiró, J., 2001, "Non-Linear Particle Tracking for High-Order Elements", *Journal of Computational Physics*, Vol. 172, pp. 356-380.

Doorly, D., Sherwin, S.J., Franke, P., Peiró, J., 2002, "Vortical Flow Structure Identification and Flow Transport in Arteries", *Computer Methods in Biomechanics and Biomedical Engineering*, In press.

Karniadakis, G., Sherwin, S.J., 1999, "Spectral hp Element Methods for CFD", *Oxford University Press.*

Khalifa, A.M.A., Giddens, D.P., 1981, "Characterization and Evolution of Post-Stenotic Flow Disturbances", *Journal of Biomechanics*, Vol. 14, No. 5, pp. 279-296.

Womersley, J.R., 1955, "Method for the Calculation of Velocity, Rate of Flow and Viscous Drag in Arteries when the Pressure Gradient is Known", *Journal of Physiology*, Vol. 127, pp. 553-563

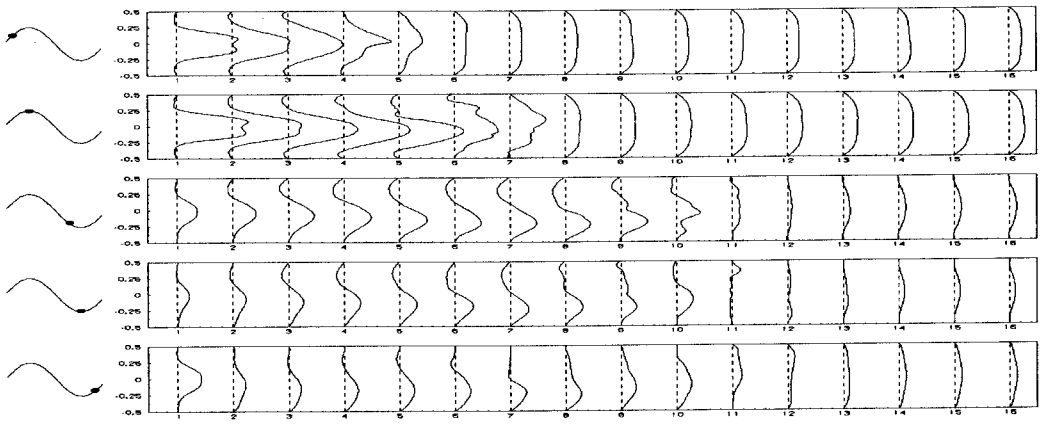

Figure 2: Axial velocity profiles for pulsatile flow through the circular stenosis at different phases during the cycle. The x-axis indicates axial location of the profiles (in units of vessel diameter downstream from the stenosis throat).

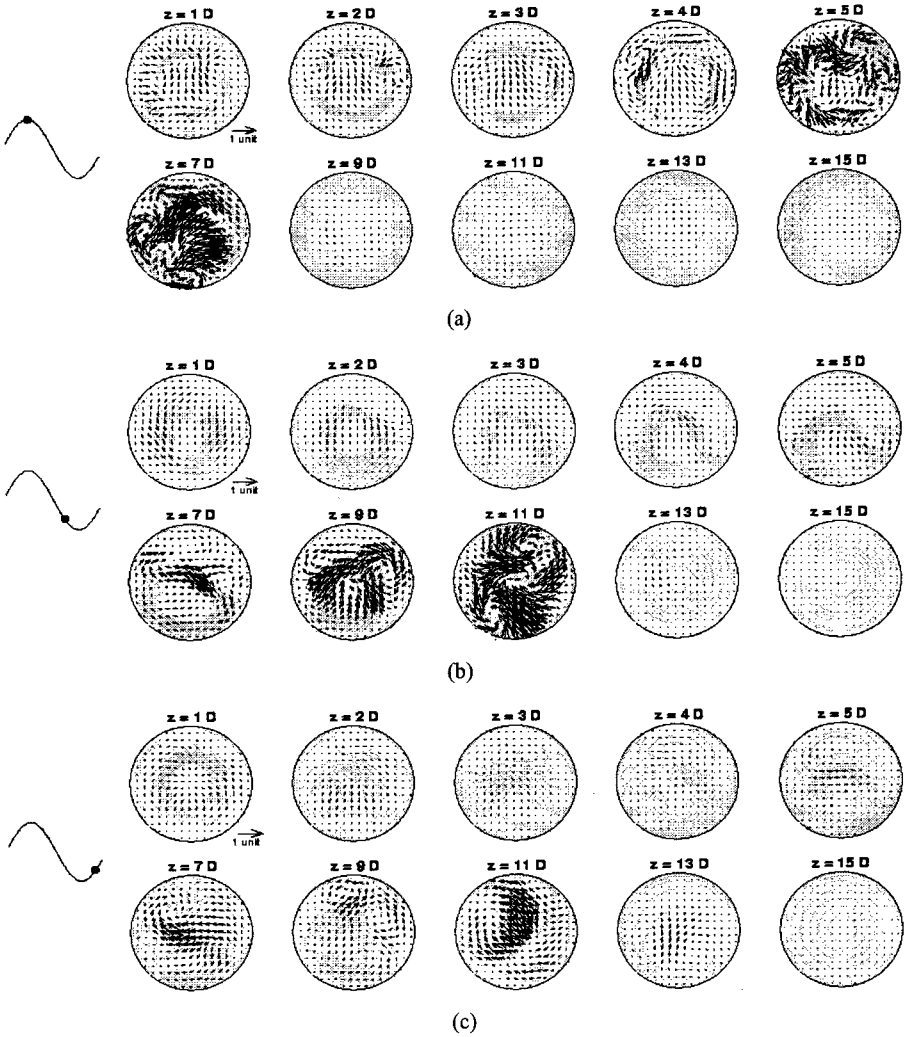

Figure 3: Axial velocity (z-velocity) contours and corresponding in-plane (x-y) velocity vectors at different slices downstream of the stenosis throat, the axial location being indicated in terms of vessel diameter.

Figure 4: Transport of marker particle rings through the circular stenosis. The thick, solid ring and the thin ring correspond to ¼ and ¾ the main vessel diameter, respectively. The rings are released during the phase indicated.

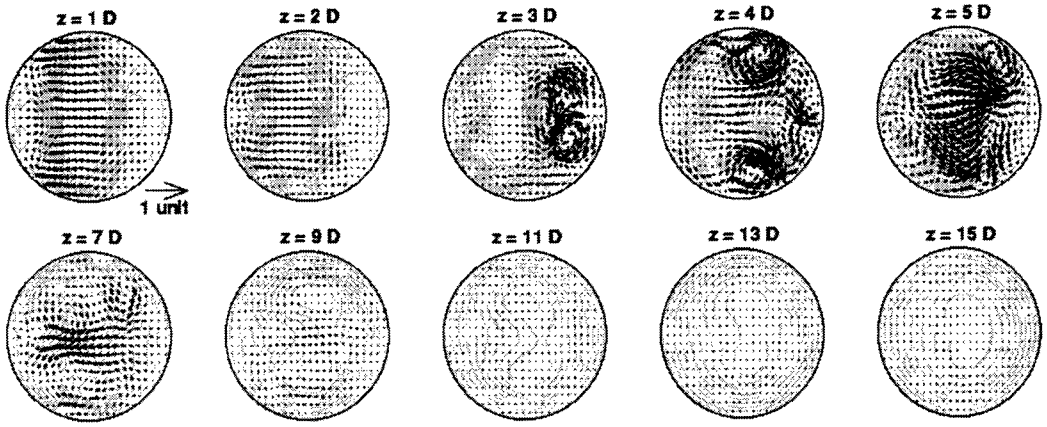

Figure 5: Axial velocity (z-velocity) contours and corresponding in-plane (x-y) velocity vectors for the elliptic stenosis. Contours are shown at different slices downstream of the stenosis throat, the axial location being indicated in terms of vessel diameter.

Figure 6: Transport of marker particle rings through the elliptic stenosis. The thick, solid ring and the thin ring correspond to ¼ and ¾ the main vessel diameter, respectively.

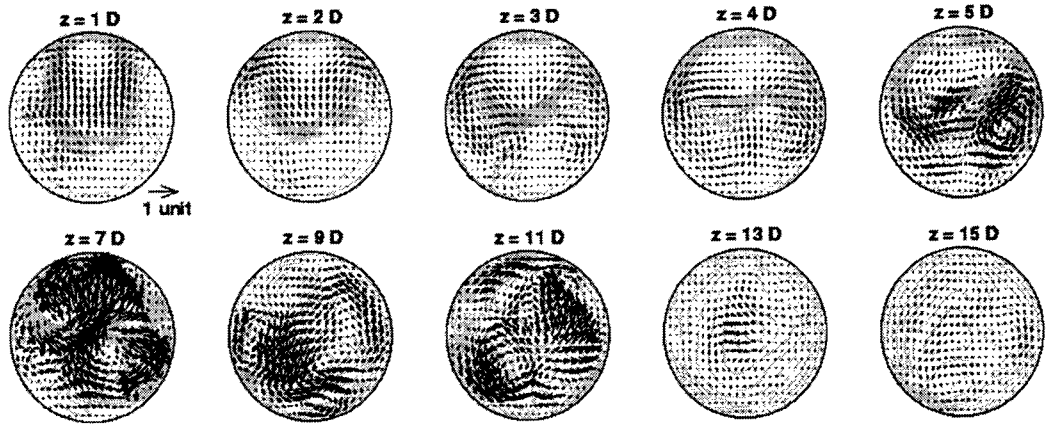

Figure 7: Axial velocity (z-velocity) contours and corresponding in-plane (x-y) velocity vectors for the asymmetric stenosis. Contours are shown at different slices downstream of the stenosis throat, the axial location being indicated in terms of vessel diameter.

Figure 8: Transport of marker particle rings through the asymmetric stenosis. The thick, solid ring and the thin ring correspond to ¼ and ¾ the main vessel diameter, respectively.